ACS APPLIED MATERIALS & INTERFACES

Research Article

www.acsami.org

Highly Flexible and Planar Supercapacitors Using Graphite Flakes/Polypyrrole in Polymer Lapping Film

C. Justin Raj,[†] Byung Chul Kim,[†] Won-Je Cho,[†] Won-gil Lee,[†] Sang-Don Jung,[‡] Yong Hee Kim,[‡] Sang Yeop Park,[§] and Kook Hyun Yu*[,†]

[†]Department of Chemistry, Dongguk University—Seoul, Jung-gu, Seoul 100715, South Korea

[‡]Electronics and Telecommunications Research Institute, Synapse Device Creative Research Centre, 218 Gajeong-ro, Yuseong-gu, Daejeon 305-700, South Korea

[§]Department of Ceramic Engineering, Gangneung-Wonju National University, Gangneung 210702, South Korea

Supporting Information

ABSTRACT: Flexible supercapacitor electrodes have been fabricated by simple fabrication technique using graphite nanoflakes on polymer lapping films as flexible substrate. An additional thin layer of conducting polymer polypyrrole over the electrode improved the surface conductivity and exhibited excellent electrochemical performances. Such capacitor films showed better energy density and power density with a maximum capacitance value of 37 mF cm^{-2} in a half cell configuration using 1 M H_2SO_4 electrolyte, 23 mF cm^{-2} in full cell, and 6 mF cm^{-2} as planar cell configuration using poly(vinyl alcohol) (PVA)/phosphoric acid (H_3PO_4) solid state electrolyte. Moreover, the graphite nanoflakes/polypyrrole over polymer lapping film demonstrated good flexibility and cyclic stability.

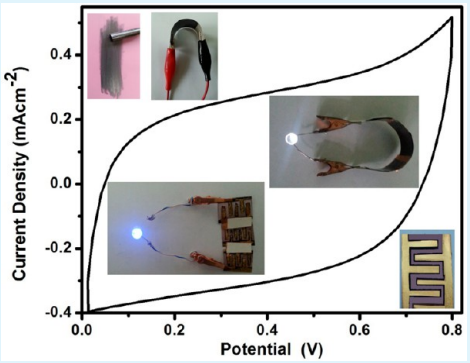

KEYWORDS: *supercapacitor, conducting polymer, graphite nanoflakes, flexible electrode, impedance spectroscopy*

INTRODUCTION

Recent advances in electronics have peaked in flexible, bendable electronic equipment such as wearable devices, foldable/rollup displays, wireless sensors, smart cards, and flexible mobile phones.[1−3] These flexible electronics require high-performance energy storage systems that have to be lightweight, ultrathin, flexible, wearable, and even foldable and rollable.[4,5] However, commercially available energy storage systems such as batteries and supercapacitors are not applicable for flexible electronics due to their significant weight, rigidity, and bulkiness. Therefore, a growing demand for lightweight and ultrathin energy storage devices, and in particular flexible batteries and supercapacitors, is expected to require flexible devices.[6,7] Among these, flexible supercapacitors (SCs) have attracted much attention due to their higher power density, longer operating lifespan than batteries, and higher energy density than dielectric capacitors.[8] SCs have been classified into electrochemical double-layer capacitors (EDLCs), that use double-layer capacitance arising from the separation of charge at the interface between the electrode/electrolyte, and pseudocapacitors, which utilize fast faradaic redox reactions that occur on the surface or in the bulk of materials.[9,10] Another interesting category is hybrid SCs, which combine the mechanism of both EDLCs and pseudocapacitors and exhibit excellent energy storage properties.[11]

Generally, for the fabrications of hybrid SC electrodes the carbon surface was modified with redox materials like transition metal oxides, hydroxides, or sulfides, or with conducting polymers.[12,13] Transition metal compounds like RuO_2,[14] NiO,[15] MnO_2,[16] CoS,[17] $Ni(OH)_2$,[18] etc., in composites with carbon nanostructures, were demonstrated as potential electrode materials for supercapacitor applications. The low conductivity and use of expensive materials are the main drawbacks of these metal oxide composites. Interestingly, the composite materials based on carbon nanostructures and conducting polymers are even promising since they can combine two relatively cheap materials to gain large pseudocapacitance with better conductivity and mechanical strength.[19,20] In addition to this the polymer/carbon composite is a promising strategy for the fabrications of flexible SCs as compared to other composite materials owing to their easy processing, mechanical flexibility, and compatibility. Several composites based on conducting polymers like polyaniline (PANI),[21] polypyrrole (PPy),[22] and poly[3,4-ethylene dioxythiophen] (PEDOT)[23] with carbon nanostructures were extensively studied. Among these polymers, polypyrrole is a potential material that exhibits high conductivity, good stability in water and air, ease of processing, and relatively low cost. Polypyrrole/carbon composite materials such as carbon black/polypyrrole,[24] carbon nanotubes/PPy,[25] carbon onion/PPy,[22]

Received: March 8, 2015
Accepted: May 26, 2015
Published: May 26, 2015

 © 2015 American Chemical Society

DOI: 10.1021/acsami.5b02070
ACS Appl. Mater. Interfaces 2015, 7, 13405−13414

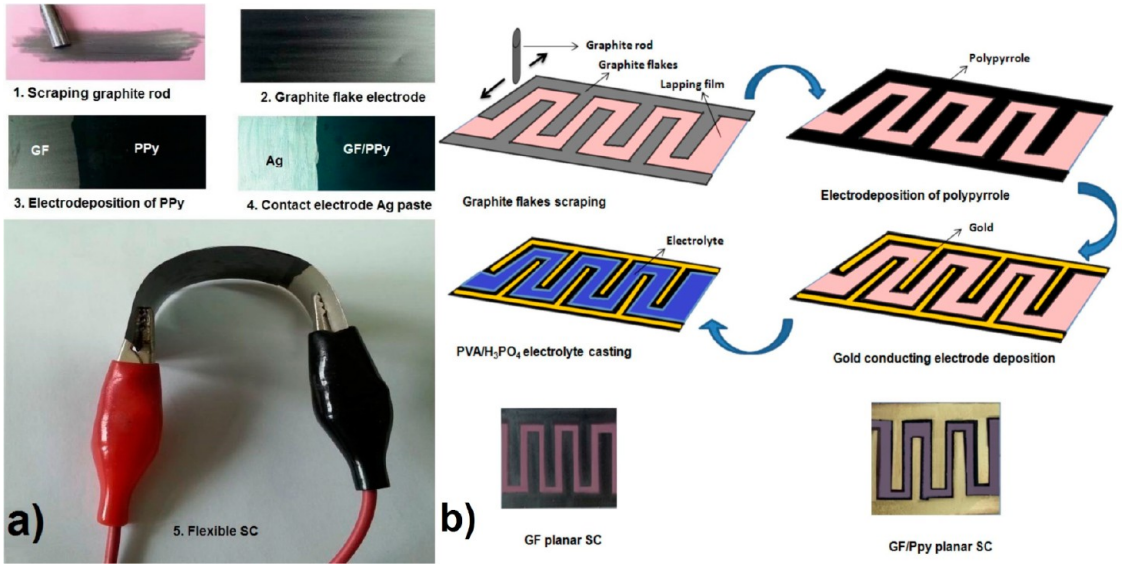

Figure 1. (a) Photographic demonstration of electrodes and SC fabrication steps. (b) Fabrication steps of planar SC and the photograph of SCs with and without gold electrode.

graphene/PPy,[26] etc. have been reported as effective SC electrode materials and have achieved good specific capacitance and electrochemical performance.

The fabrication of flexible SCs required a current collector (substrates) which has to be highly flexible, cost-effective, stable against corrosive electrolyte, and easy to fabricate. Recently, great efforts have been made to fabricate flexible supercapacitors employing various types of carbon materials, metal oxides, and conductive polymers into a number of flexible substrates, such as plastics, textile fibers, metal wires, papers, and cellulose.[6,27−30] Generally, complicated fabrication techniques have been adopted for the preparation of these SCs, while the flexible substrate needs to be reliable, simple, stable, and cost-effective. However, flexible substrates often require gold coating, which increases the overall cost of fabrication. Fiber based substrates suffer from complicated fabrication methods, complex structures, and relatively low flexibility, which could be obstacles for the overall performance of flexible SCs.[31,32] Carbon based nanostructures like CNTs, graphite sheets, graphene, etc. are attractive materials for SC substrate fabrications. Since it is highly stable in any type of aqueous electrolyte and very flexible, the same material could potentially act as an active material as well as current collector.[33]

In this present work, we report a simple design for the fabrication of flexible supercapacitor electrodes and their characterization. The flexible electrodes were constructed by scraping a graphite rod over a commercially available polymer lapping film having appropriate grit (4000; particle size 3 μm). A thin layer of conducting p-toluene sulfonate (pTS)-doped polypyrrole (PPy) was galvanostatically polymerized over the graphite coated lapping film to form a hybrid flexible SC electrode. Such capacitor sheets showed a maximum capacitance of 37 mF cm^{-2} in a half cell using 1 M H_2SO_4 electrolyte, 23 mF cm^{-2} in full cell, and 6 mF cm^{-2} as planar cell configuration using poly(vinyl alcohol) (PVA)/H_3PO_4 solid state electrolyte.

EXPERIMENTAL METHODS

Graphite Flake/Polypyrrole Electrode Fabrications. Aluminum oxide bonded polyester lapping films of grit 1500, 4000, 8000, and 15000 were purchased from Thorlabs Japan Inc. Initially the smooth surface of a graphite rod (Dong Lin Co. Ltd., Korea) was gently scraped over the clean surface of lapping film until a uniform graphite layer formed. The film was then rinsed with absolute ethanol and deionized (DI) water to remove the loosely bonded graphite flakes, leaving behind ca. 0.3 mg cm^{-2} of GFs coated over 4000 grit lapping film. A conducting polymer layer (pTS-doped polypyrrole) was deposited galvanostatically using ZIVE-SP2 electrochemical workstation in a three electrode arrangement containing a working electrode of GF coated lapping film, a carbon mesh counter electrode, and a Ag/AgCl reference electrode. The deposition was performed in an aqueous solution containing 0.1 M pyrrole and 0.1 M *p*-toluene sulfonic acid sodium salt, at a constant current density of 2 mA cm^{-2} for 3 min. The resultant GF/PPy film was rinsed with DI water and dried at 60 °C. The mass of the PPy film deposited over the GF coated lapping film was ∼0.25 mg cm^{-2}. Finally, a conducting silver paste was painted over the appropriate portion of the GF/PPy flexible electrode to act as a contact electrode.

Fabrication of Flexible Solid State Supercapacitors. Poly(vinyl alcohol) (PVA)/phosphoric acid (H_3PO_4) electrolyte was prepared by the solvent casting method. PVA (1 g) was dissolved in DI water (10 mL) at 90 °C with vigorous stirring until the solution became clear, and then 1.5 g of H_3PO_4 was added into the hot solution and stirred at room temperature overnight. The flexible solid state supercapacitor was fabricated by immersing the selected area (1 × 1 cm^2) of GF/PPy lapping film in the PVA/H_3PO_4 electrolyte for 5 min, and then the electrode was left for 4 h at 40 °C to form a less aqueous electrolyte film. Finally, the supercapacitor was assembled by sandwiching the two electrodes under pressure. The device was finally placed in a vacuum oven at 60 °C to remove excess water.

Fabrication of Planar Supercapacitors. The 2D patterned planar GF electrodes were fabricated by gently scraping the smooth surface of a graphite rod over the appropriate area of the polymer lapping film (size ∼2 × 1.5 cm^2) as represented in Figure 1b. The gap between the two adjacent electrode fingers is ∼1.6 mm. A layer of pTS-doped polypyrrole was deposited galvanostatically over the adjacent GF electrodes separately at a constant current density of 2 mA cm^{-2} for 3 min. Then, a thin layer of gold contact electrode was coated by vacuum evaporation over the GF/PPy electrodes placing a mask between space of the electrode fingers. Finally, the spaces between the electrodes were filled with PVA/H_3PO_4 electrolyte and dried overnight in a vacuum oven at 60 °C. The bare GF planar SC was fabricated by same procedure without deposition of polypyrrole film.

DOI: 10.1021/acsami.5b02070
ACS Appl. Mater. Interfaces 2015, 7, 13405−13414

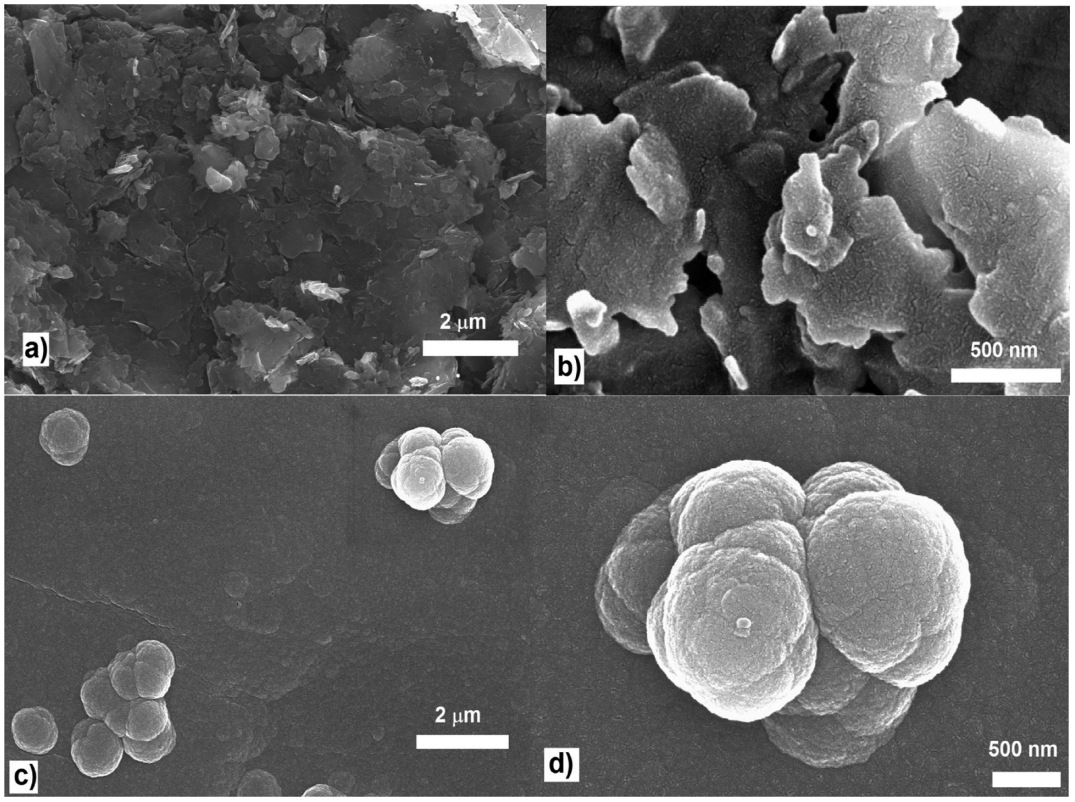

Figure 2. SEM image of GF coated 4000 grit polymer lapping film: (a) low magnification and (b) high magnification image. SEM image of GF/PPy coated 4000 grit polymer lapping film (c) low magnification and (d) high magnification image.

Characterizations and Electrochemical Measurements. The crystallinity and structure of graphite rod and GF and GF/PPy thin films were analyzed by X-ray diffraction (XRD, D/Max-2400, Rigaku) using a Cu Kα source operated at 40 kV and 30 mA in the 2θ range 10−80°. Surface morphology of thin films was revealed using field emission scanning electron microscope (FE-SEM, S-4200, Hitachi) operated at 15 kV. Transmission electron microscopy (TEM) of GF was recorded using a JEOL (Japan) model JEM-2100F microscope. Surface resistance of films was tested with a Keithley 2100 digital multimeter and four probe electrodes (Pen probe VI.I Teraleader. Inc.). Attenuated total reflectance-Fourier transform infrared spectroscopy (ATR-FTIR) measurement was performed using ATR-FTIR spectrometer (Smiths Detection). Electrochemical measurements were performed at room temperature (~25 °C) using ZIVE - SP2 (Korea) electrochemical workstation, and in three electrode configuration with a working electrode of GF or GF/PPy film, a carbon mesh counter electrode, and a 3 M KCl-Ag/AgCl reference electrode in 1 M H_2SO_4 or 1 M Na_2SO_4 aqueous electrolyte solutions.

Calculation of Area Capacitance, Energy, and Power Density. Area capacitance (C_{area}) values were calculated from CV data according to

$$C_{area} = \int i\, dV/2(A \times s \times \Delta V) \quad (1)$$

where A is the area of active material on electrodes (cm^2), s is the scan rate ($mV\ s^{-1}$), i is the voltammetric current (A), and ΔV is the potential window of the CV curve.

Area capacitance (C_{area}) values from galvanostatic charge/discharge curves were calculated according to[34]

$$C_{area} = 2 \times D_{area} \times I/V^2 \quad (2)$$

where I is the applied current (A), A is the active area of the electrodes (cm^2), D_{area} is the area under the discharge, and V is the potential window excluding IR drop (V).

The electrochemical performances of all flexible capacitors shown in Ragone plots were based on area capacitances measured using galvanostatic charge/discharge curves. The energy density and the power density of the SCs were estimated according to

$$E = 1/2 \times C_{area} V^2 \quad (3)$$

and

$$P = E/\Delta t \times 3600 \quad (4)$$

where E is the energy density ($W\ h\ cm^{-2}$), V is the operating potential (V), C_{area} is the area capacitance ($mF\ cm^{-2}$) of the SCs, P is the power density ($W\ cm^{-2}$), and Δt is the discharge time (s).

RESULTS AND DISCUSSION

Figure 1a shows the photographic account of electrode fabrication steps utilizing polymer lapping film/graphite rod and polypyrrole. Figure 1b depicts the fabrication steps of planar supercapacitors over polymer lapping film and shows the photographs of fabricated cells. Lapping sheets are similar to sand paper and have tiny aluminum oxide particles glued to a substrate of polyester with resin. In the present investigation four different types of lapping sheets of grit 1500 (12 μm Al_2O_3 particle size), 4000 (3 μm), 8000 (1 μm), and 15 000 (0.3 μm) were used as a flexible substrate. Among these, 4000 grit shows a better loading of micron to nanosized graphite flakes over the surface with a good surface conductivity. Supporting Information Figure S1a shows the scanning electron microscopy (SEM) image of the 4000 grit lapping sheet demonstrating its rough surface capable of holding several layers of graphite flakes strongly as well as uniformly.

The SEM image of graphite scraped over the 4000 grit lapping sheet (Figure 2a,b) reveals that the graphite was formed as thin micron sized sheets of 2D graphite flakes (GFs) with

DOI: 10.1021/acsami.5b02070
ACS Appl. Mater. Interfaces 2015, 7, 13405−13414

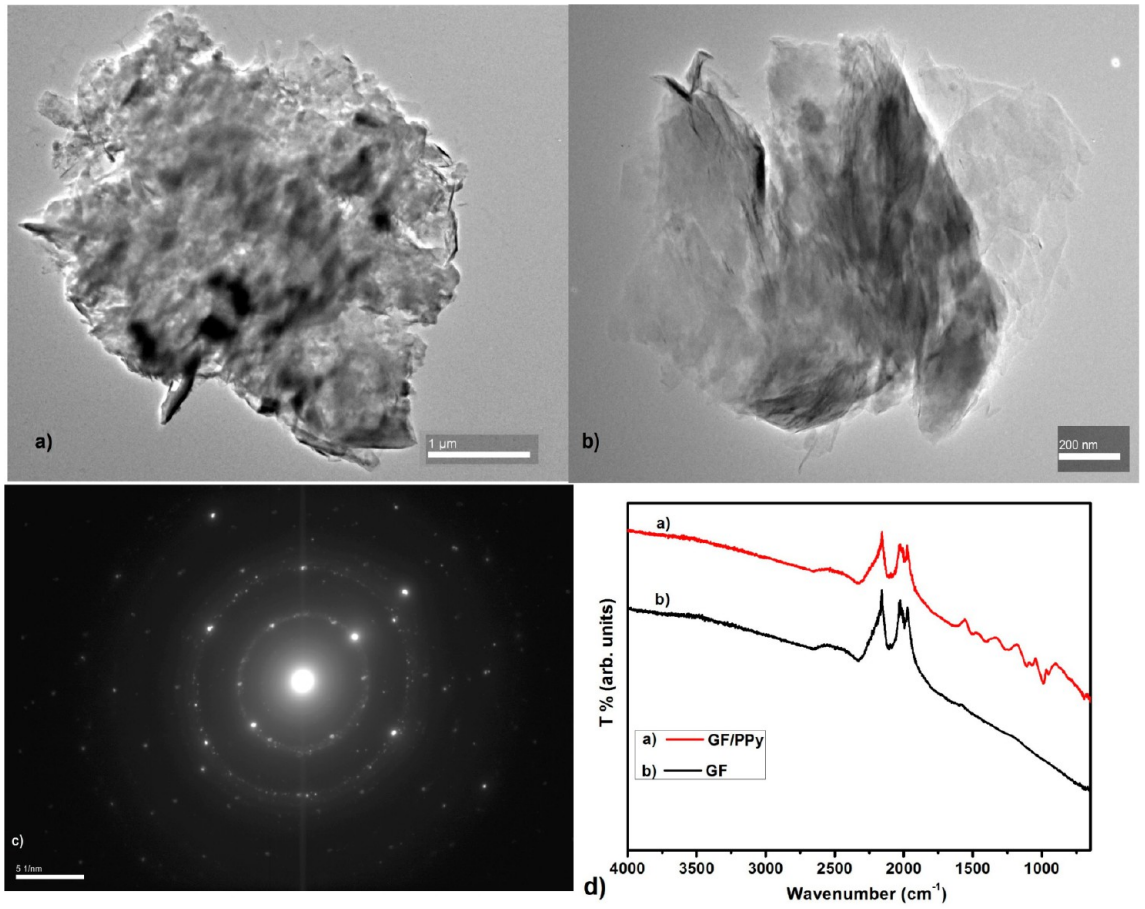

Figure 3. (a, b) TEM image of GF from 4000 grit polymer lapping film. (c) SAED pattern of graphite flakes. (d) ATR-FTIR spectra of GF and GF/PPy coated lapping film.

thickness of a few nanometers. Moreover, low-magnification SEM (Supporting Information Figure S1b) shows that the graphite forms a relatively uniform film over a large surface area on the lapping film. For 8000 and 15 000 grit lapping films only a relatively low density of graphite flakes (~0.1 and 0.04 mg of GF was coated over 8000 and 15 000 grit lapping film, respectively) are nonuniformly coated, as shown in the representative SEM image of 8000 and 15 000 grit film (Supporting Information Figure S1d,e). The surface resistance of GF coated 4000 grit film (195 Ω cm^{-2}) was much less than that of GF coated 8000 grit film (15 kΩ cm^{-2}). GF coated 1500 grit film showed a relatively low surface resistance of 150 Ω cm^{-2}; however, particles easily flaked off from the substrate due to the loading of large graphite particles (~0.8 mg), meaning that this particular material is inappropriate as a flexible substrate (Supporting Information Figure S1c). On the basis of the results of these experiments, 4000 grit lapping film was confirmed as a better flexible substrate for SC fabrication.

In order to further improve the conductivity and surface quality of GF coated films, a layer of pTS-doped polypyrrole (since it is known that the pTS dopant can improve the stability of PPy SCs)[35−37] was galvanostatically deposited at 2 mA cm^{-2} (Supporting Information Figure S2a). Figure 2c,d shows an SEM image of the PPy coated GF surface, confirming the formation of PPy film with few cauliflower-like morphologies constituted by microspherical grains which is in good agreement with the previous reports of PPy film deposited by the electro-polymerization technique.[38,39] The cross sectional SEM image of GF/PPy film shows that a nearly 5 μm thick film was coated over the lapping film surface (Supporting Information Figure S1f). Moreover, the film demonstrated a very low surface resistance of ~89 Ω cm^{-2} with a uniform coating over a large area, as shown in Supporting Information Figure S2b. A transmission electron microscopy (TEM) image was recorded for the GF obtained from the surface of 4000 grit lapping film (Figure 3a and b), which confirmed that the micron sized sheets of 2D graphite flakes resembling a few hundred graphene sheets stacked irregularly. The selected area electron diffraction (SAED) pattern of graphite flakes is shown in Figure 3c, where the diffraction spots indicate the good crystallinity of the GF. Furthermore, Supporting Information Figure S3a shows the X-ray diffraction pattern of graphite, polymer lapping film, GF, and PPy coated GF films. The prominent diffraction peaks of (002) and (004) are assigned to the hexagonal structure of graphite crystals and are in good agreement with the JCPDS card (no. 41-1487). The XRD pattern of lapping film shows the diffraction peaks of Al_2O_3 crystallites glued in the lapping film surface (JCPDS 10-0123). The diffraction peak at 25.58° of Al_2O_3 was reflected in both GF and GF/PPy films with a broad pattern; this peak broadening might be the reflection from the (002) phase of thin graphite flakes. Moreover an additional small peak was observed at 54.5° for both GF and GF/PPy coated films which matches the (004) diffraction of the bare graphite sample. In GF/PPy coated films no diffraction peaks due to PPy were observed, likely due to less crystallinity of the PPy layer

DOI: 10.1021/acsami.5b02070
ACS Appl. Mater. Interfaces 2015, 7, 13405−13414

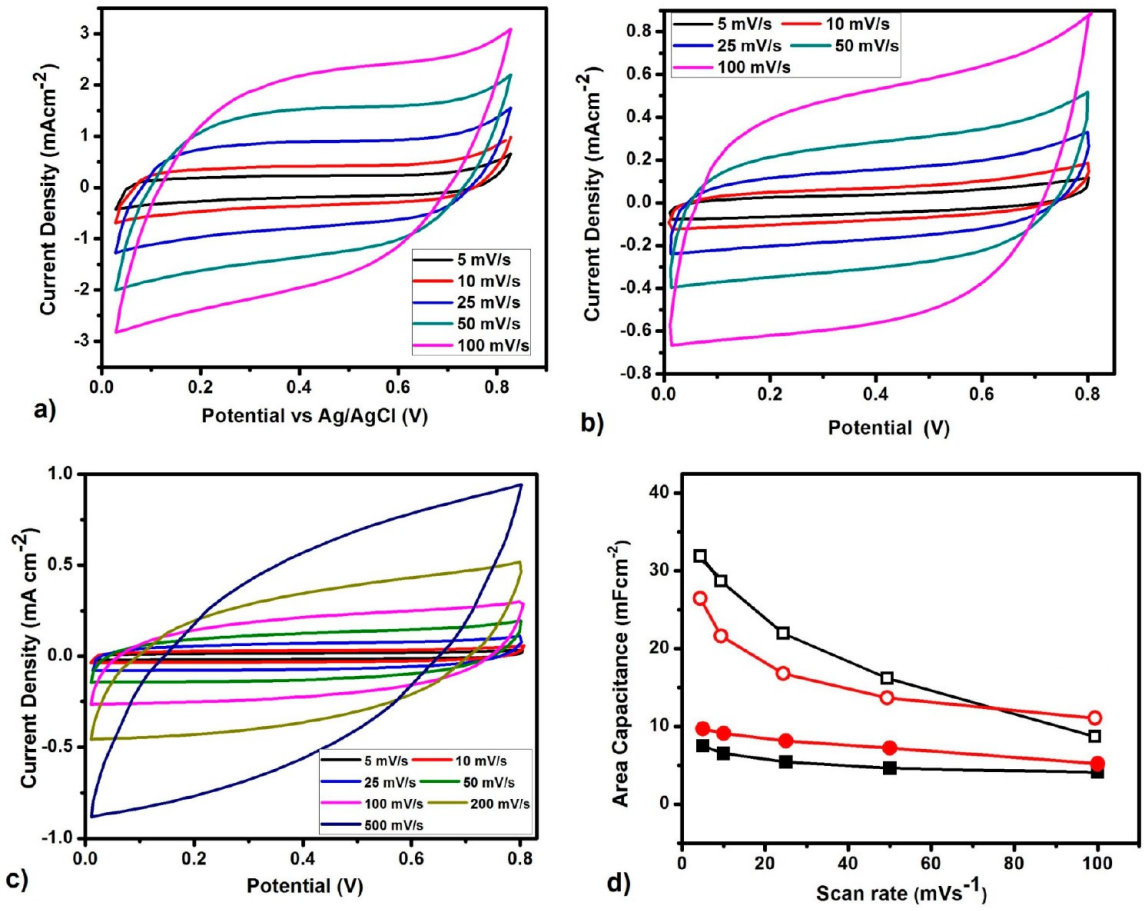

Figure 4. (a) CV curves of GF/PPy electrode in 1 M H_2SO_4 electrolyte at different scan rates. (b) CV curves of GF/PPy flexible full cell for various scan rates. (c) CV curves of GF/PPy planar cell for various scan rates. (d) Evolution of the area capacitance versus scan rate for GF, GF/PPy electrodes in 1 M H_2SO_4 electrolyte and GF, GF/PPy flexible full cells.

compared with the GF and Al_2O_3 particles. To ensure the presence PPy layer the ATR-FTIR spectrum was recorded for the surface of GF and GF/PPy coated films (Figure 3d). The few broad absorption peaks observed in GF film at 2320, 2011, 1994, and 1921 cm^{-1} are attributed to the vibrations of O—H, C—H, and C═O of the impurities present in the graphite surface. From the spectrum of the GF/PPy film few additional absorption peaks are observed due to the presence of the PPy layer. The broad band at 1650 cm^{-1} present in the GF/PPy film is attributed to the fundamental vibration of pyrrole ring. The peaks at 1510 and 989 cm^{-1} shows the stretching modes of PPy rings. The absorption band at 1412 and 1050 cm^{-1} is an indication of the ═C—H in plane vibration of PPy, and the band at 1266 and 1110 cm^{-1} can be ascribed as the C—N stretching vibration or C—H in plane deformation mode.[22,37,40] The ATR-FTIR spectrum of the bare lapping film is shown in Supporting Information Figure S3b representing the vibration of functional groups present in the polyester substrate. These peaks were not observed in both GF and GF/PPy coated lapping film revealing that the presence GF and PPy masks the absorption peaks of substrate.

Electrochemical capacitance behavior of the flexible GF and GF/PPy substrates was measured by cyclic voltammetry (CV) and galvanostatic charge/discharge tests in 1 M H_2SO_4 in a three electrode configuration and employing PVA/H_3PO_4 solid polymer electrolyte in symmetric full cell (FC) and planar cell (PC) configuration. Figure 4a shows the CV curves of a GF/PPy electrode in 1 M H_2SO_4 at various scan rates. The CVs show a nearly rectangular shape illustrating an excellent electrochemical performance and reflected a maximum area capacitance of 32 mF cm^{-2} at a scan rate of 5 mV s^{-1}, which is much higher than the area capacitance of a bare GF based flexible electrode (5.9 mF cm^{-2}) at the same scan rate (CVs shown in Supporting Information Figure S4a). This observation reveals that a layer of PPy over GF effectively reinforced the surface state and remarkably improved electrochemical performance with additional pseudocapacitance originating from the PPy film. Moreover, CVs were measured for both GF and GF/PPy flexible electrodes in 1 M Na_2SO_4 electrolyte (Supporting Information Figure S4b,c). These electrodes showed area capacitance values of 2.9 and 26.4 mF cm^{-2}, respectively, at 5 mVs^{-1} scan rate, affirming comparable capacitance values in neutral aqueous electrolyte. Additionally, CVs of various grit (1500, 8000, and 15 000) GF coated lapping sheets were measured in 1 M H_2SO_4 electrolyte and compared with 4000 grit lapping film based electrode. The obtained CVs at 100 mV s^{-1} scan rate are presented in Supporting Information Figure S5a, and the electrodes exhibit area capacitances of 1.67 mF cm^{-2} for 1500 grit, 0.22 mF cm^{-2} for 8000 grit, and 0.084 mF cm^{-2} for 15 000 grit. The 4000 grit lapping film electrode showed much higher area capacitance (4.07 mF cm^{-2}) and was thus confirmed as a promising flexible substrate for the present study.

DOI: 10.1021/acsami.5b02070
ACS Appl. Mater. Interfaces 2015, 7, 13405−13414

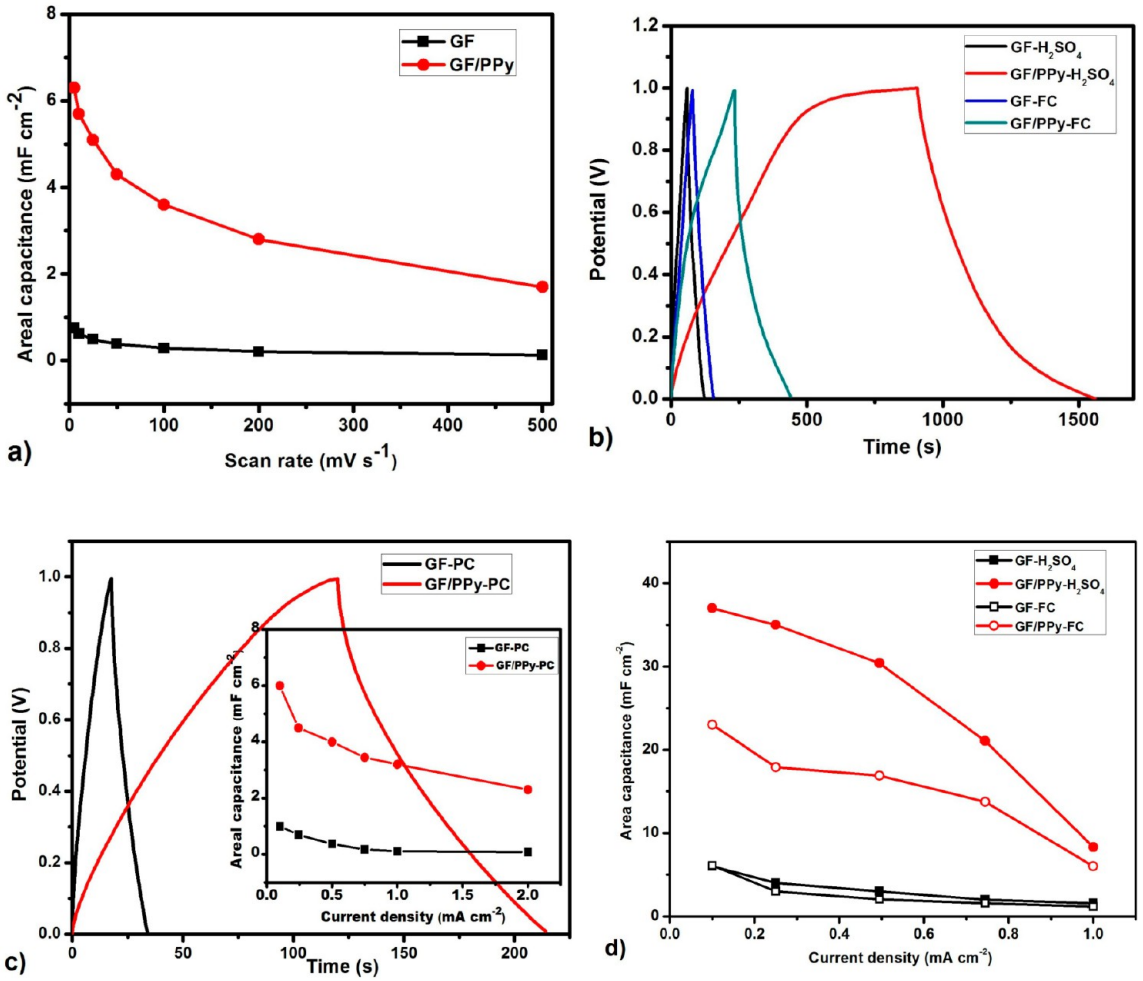

Figure 5. (a) Variation of area capacitance versus scan rate for GF, GF/PPy planar SCs. (b) Galvanostatic charge/discharge curves of GF, GF/PPy electrodes in H_2SO_4 electrolyte, and flexible full cells at a discharge current density 0.1 mA cm^{-2}. (c) Galvanostatic charge/discharge curves of GF, GF/PPy planar cells at 0.1 mA cm^{-2} discharge current density; inset shows the variation of area capacitance of planar cells with respect to applied discharge current densities. (d) The variation of area capacitance of the GF and GF/PPy SCs with respect to the various discharge current densities.

With a view to applications, flexible electrodes were studied by employing symmetric full cell configuration using PVA/H_3PO_4 solid polymer electrolyte. The resultant CV curves for GF/PPy at various scan rates are shown in Figure 4b (GF CVs in Supporting Information Figure S4d). Similar to the corresponding half-cell the CV shows a nearly rectangular shape representing ideal capacitance behavior of the SCs. Area capacitances were calculated to be 7.7 mF cm^{-2} and 26 mF cm^{-2} for GF and GF/PPy flexible solid state SCs, respectively. Moreover, the specific capacitance of the GF, GF/PPy, and PPy was comparatively studied for both cell configurations to ensure the enhancement of capacitance value. Supporting Information Figure S6a,b shows resultant CV curves of half and full cell for GF, GF/PPy, and PPy measured at the 25 mV s^{-1} scan rate. The specific capacitance were calculated to be 6 and 20 F g^{-1} for GF (0.3 mg) half and full cell, and 138 and 80 F g^{-1} for bare PPy (0.25 mg) half and full cell. The combination of this to GF and PPy layers shows a specific capacitance values of 65 and 47 F g^{-1}, respectively, for both half and full cell configuration. From this observation it is clear that the layer of PPy over GF film effectively reinforces the surface state of the electrode by enhancing the conductivity, improving the hydrophilicity of the surface, and providing additional pseudocapacitance.

More simplified configurations of SCs the two-dimensional (2D) planar type of supercapacitors were fabricated. Since the 2D in plane pattern takes advantage of the thin layered and flat morphology of graphitic flakes, it is ideal for 2D devices. Also, this design could offer the entire device advantages such as being much thinner, lighter, and more flexible. Moreover, in 2D design the usage of the spacer can be eliminated due to the 2D transport of electrolytic ions between the electrodes.[41−43] Figure 4c shows the resultant CV curves of the GF/PPy planar cell for different scan rates (GF CVs in Supporting Information Figure S5b). The CV shows a rectangular voltammogram at lower scan rates with maximum specific capacitance of 6.5 mF cm^{-2} and 1 mF cm^{-2} at 5 mV s^{-1} scan rate for GF/PPy and GF planar SCs, respectively. Even at a fast scan rate of 500 mV s^{-1} the planar cells still delivered an area capacitance of 2 mF cm^{-2}; this shows that the PC can charge and discharge rapidly up to 500 mV s^{-1} while maintaining good capacitance characteristics of high instantaneous power.[44] The variation of specific capacitance with respect to scan rate is shown in Figure 4d and Figure 5a. From these plots, GF/PPy based SCs show a large drop in area capacitance with increasing scan rate compared with that of bare GF based SCs. Although at high scan rate the PPy layer over GF can effectively mask the active sites of graphite flakes and the electrochemical reaction only

DOI: 10.1021/acsami.5b02070
ACS Appl. Mater. Interfaces 2015, 7, 13405−13414

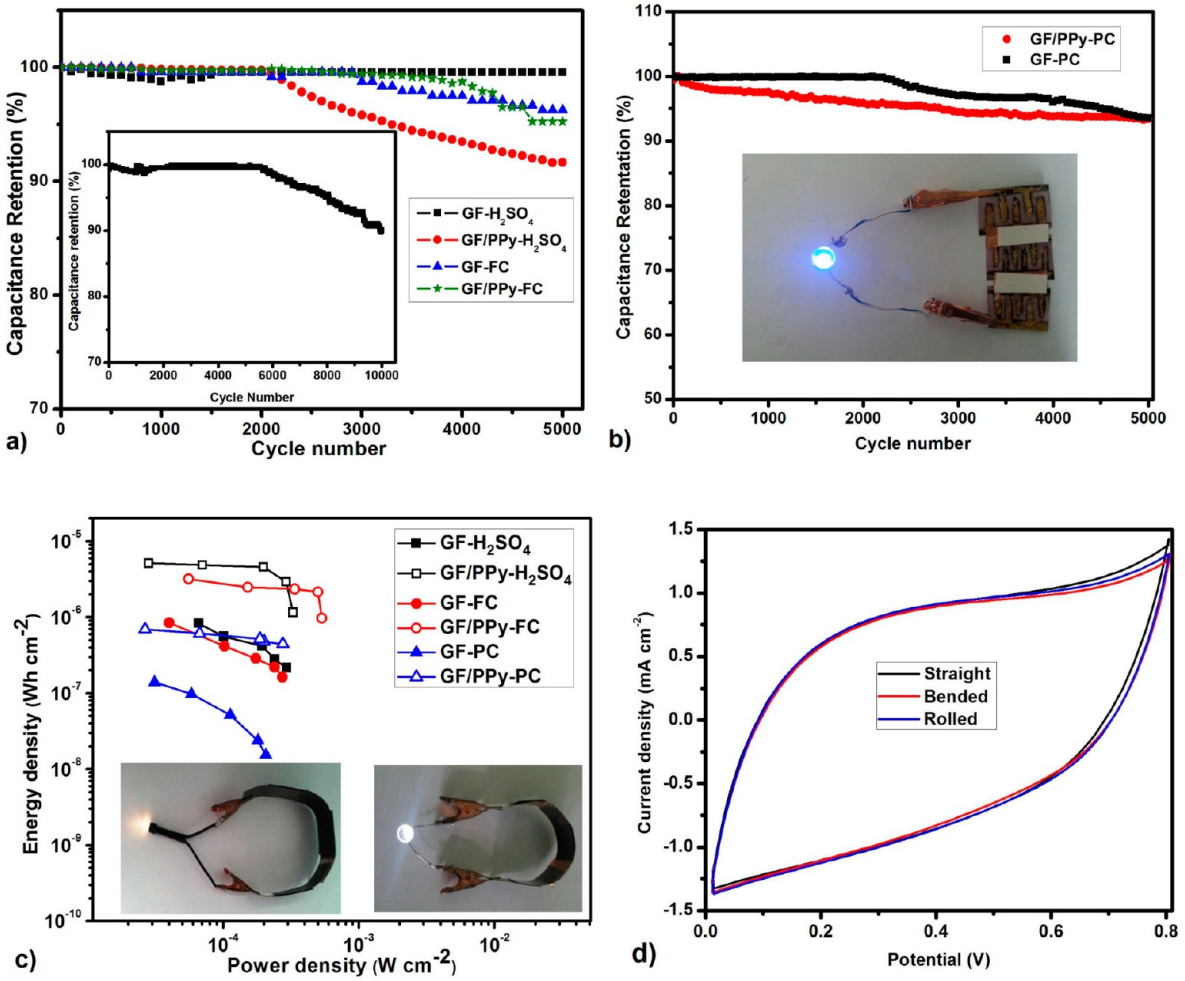

Figure 6. (a) Cycling stability of the GF and GF/PPy in H_2SO_4 electrolyte and GF and GF/PPy full cells for 5000 cycles (inset shows the extended cyclic stability of GF in H_2SO_4 electrolyte for 10 000 cycles revealing the good stability of GF in 4000 grit polymer lapping film). (b) Cycling stability of the GF and GF/PPy planar cells for 5000 cycles (inset shows the demonstration of serially connect planar cells glowing a blue LED (2.2 V, 10−20 mA)). (c) Ragone plot for GF and GF/PPy electrodes, full cells, and planar cells; the inset picture showing that three SCs in series can lighten up a warm and pure white LED (3 V, ∼10−20 mA) powered by 30 s charged SCs. (d) CV curves of the flexible GF/PPy full cell at different measurement conditions like straight, bent, and rolled state at 100 mV s^{-1} scan rate.

occurs at the PPy surface, GF SCs show nearly constant capacitance values representing the current accumulation energy storage process at the active sites of GF.[45]

Further, the electrochemical performance was evaluated via galvanostatic charge/discharge tests using various discharge current densities (0.5−2 mA cm^{-2}) over the potential window 0−1 V. Charge/discharge profiles of GF and GF/PPy SCs at a constant discharge current density of 0.1 mA cm^{-2} are shown in Figure 5b,c. The corresponding charge/discharge curves at various discharge current densities of individual SCs are presented in Supporting Information Figure S7a−f. The curves for GF based SCs display a typical symmetrical triangular shape revealing that the capacitance originates from the electric double layer at GF/electrolyte interfaces. In contrast GF/PPy presents a slightly tilted triangle resembling those reported for hybrid SCs,[46,47] which confirms the overall enhancement of electrochemical performance of GF/PPy SCs due to the influence of the thin PPy layer. Figure 5b,c (inset) depicts the variation of calculated area capacitance with respect to the applied discharge current densities. The GF/PPy SC shows excellent area capacitance in both half, full, and planar cell forms, namely, 10−37 mF cm^{-2} in 1 M H_2SO_4 electrolyte, 9−23 mF cm^{-2} as flexible full cell, and 3−6 mF cm^{-2} as planar cell for discharge current densities ranging from 1 to 0.1 mA cm^{-2}. At the same time the bare GF SC shows 2−6 mF cm^{-2} in 1 M H_2SO_4 electrolyte, 2−7 mF cm^{-2} as flexible solid state full cell, and 0.11−1 mF cm^{-2} as planar supercapacitor. Area capacitance values of the flexible GF/PPy SCs prepared here are comparable or higher compared to those of recently reported fiber and paper based flexible SCs (see Supporting Information Table S1). Moreover the capacitance value of 7 mF cm^{-2} for bare GF based flexible SC is higher than area capacitance values (2.3 and 1.13 mF cm^{-2}) reported for paper/graphite based flexible SCs.[48]

The cyclic stability of flexible GF and GF/PPy SCs were investigated by continuous charge/discharge measurements over 5000 cycles (Figure 6a) at a constant current density of 1 mA cm^{-2}. The GF/PPy SC showed excellent cycling stability with 91% and 95.2% retention of initial area capacitance values after 5000 cycles in H_2SO_4 and PVA/H_3PO_4 electrolytes, respectively. Flexible GF electrodes in H_2SO_4 and PVA/H_3PO_4 electrolytes showed even better cyclic stability with 99.5% and 96.5% area capacitance retention, respectively, after 5000 cycles. This may be attributed to better stability of GF against acidic

DOI: 10.1021/acsami.5b02070
ACS Appl. Mater. Interfaces 2015, 7, 13405−13414

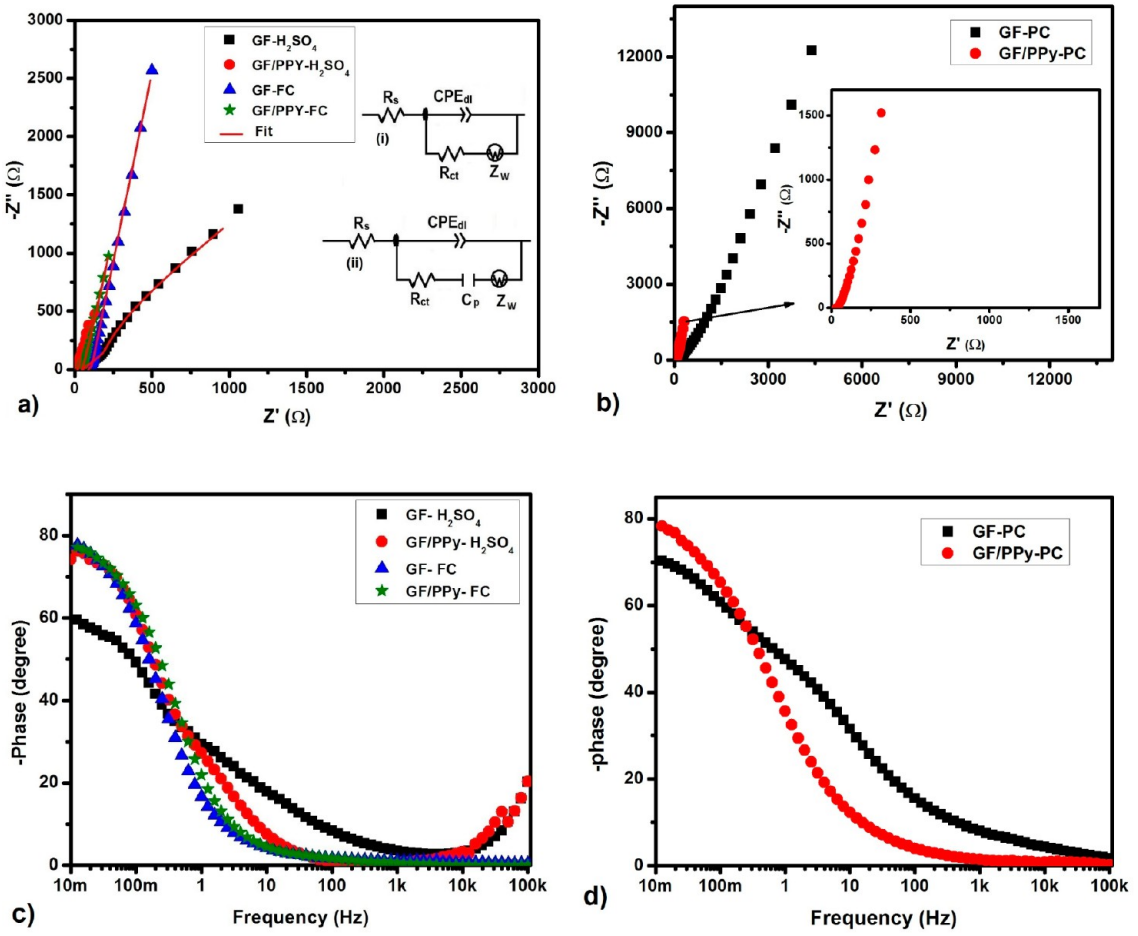

Figure 7. (a) Nyquist plots for the GF and GF/PPy flexible supercapacitors (inset shows the equivalent circuits of fit). (b) Nyquist plots for the GF and GF/PPy planar SCs (inset shows the magnified plot of GF/PPy planar cell. (c) Bode plots for the GF and GF/PPy flexible supercapacitors. (d) The Bode plots of GF/PPy planar SCs.

electrolytes compared to the polymer layer. Furthermore, the cyclic test was extended for a GF film in 1 M H_2SO_4 to 10 000 cycles, with the resultant plot depicted in the inset of Figure 6a. The electrode showed only ~9.8% capacitance loss, displaying the excellent stability of GF electrode in polymer lapping film. Figure 6b shows the cyclic stability of planar GF and GF/PPy SCs; the SCs showed good cyclic stability with ~93.5 and 93.3% retention of the initial area capacitance values after 5000 cycles of charge/discharge cycles.

Figure 6c shows the Ragone plot (energy density vs power density) of GF and GF/PPy SCs. The energy density of flexible SCs decreases from 3.194×10^{-6} to 9.72×10^{-7} W h cm^{-2} (GF/PPy-FC) and from 8.42×10^{-7} to 1.63×10^{-7} W h cm^{-2} (GF-FC), while the power density increases from 0.0056 to 0.05 mW cm^{-2} (GF/PPy-FC) and from 0.004 to 0.027 mW cm^{-2} (GF-FC). These results are comparable to the power and energy densities of recently reported SCs fabricated using paper and fiber based substrates.[29,49] Moreover the energy densities of planar SCs decrease from 6.97×10^{-7} to 4.44×10^{-7} W h cm^{-2} and the corresponding power densities increases from 0.0026 to 0.028 mW cm^{-2}. Furthermore, the performance of flexible GF/PPy SC was verified by assembling three flexible SCs in series, charging for 30 s, and then successfully powering warm white (2.5−3 V, 10−20 mA) and pure white (3 V, 10−20 mA) light-emitting diodes (LEDs) of 5 mm diameter (inset of Figure 6c). LEDs emitted very bright light after 2 min and even glowed after 5 min, demonstrating the good power and energy density of the fabricated flexible SCs. The inset of Figure 6b displays the demonstration of the GF/PPy planar SCs; a series connection of 3 charged cells can effectively light up a blue LED (2.2 V, 10−20 mA) of 5 mm diameter. In addition, the flexibility of a GF/PPy FC was probed using CV measurements while bent and rolled. Figure 6d shows that the areas under the curves during bending and rolling were almost identical (just ~1.5−2% difference) to that measured under a normal straight condition.

Electrochemical impedance spectroscopy (EIS) analysis was performed in the frequency range 10 mHz to 100 kHz at 0 V potential bias to further evaluate the electrochemical behavior of SCs. The obtained Nyquist plots for GF, GF/PPy half, full, and planar cells are shown in Figure 7a,b. Also, the plots were analyzed using ZView software on the basis of the electrical equivalent circuits shown in the inset of Figure 7a. The bulk solution resistance is represented as R_s, the double-layer capacitance as CPE_{dl}, and R_{ct} is the charge transfer resistance across the electrode/electrolyte interface. The spike at lower frequency of the plots exhibits an angle between 45° to 90° relative to the real axis, representing the diffusion control process of the electrode, which was fitted with a Warburg element Z_w. For GF/PPy SCs an additional CPE_p representing the pseudocapacitance of the electrodes was added to the

DOI: 10.1021/acsami.5b02070
ACS Appl. Mater. Interfaces 2015, 7, 13405−13414

circuit (ii). The best fitted values of the SCs are presented in Table 1.

Table 1. EIS Fit Results of GF and GF/PPy SCs

SCs	R_s [Ω]	R_{ct} [Ω]	C_{dl} [F/cm^2]	Z_w [Ω]	C_p [F/cm^2]
GF-H_2SO_4	46.95	11.69	0.0021	1144	
GF/PPy-H_2SO_4	14.3	3.23	0.0086	151.2	0.0567
GF-FC	88.95	12.51	0.0012	68.43	
GF/PPy -FC	31.3	3.017	0.0077	39.46	0.0223
GF-PC	85.6	24.59	0.00012	5177	
GF/PPy-PC	34.5	11.31	0.00036	499	0.0173

Overall resistance values of the SCs are the combination of R_s with R_{ct} and limited resistance values,[46] which were found to be relatively low for GF/PPy SCs at 17.5, 34.3, and 45.8 Ω cm^{-2} for half, full, and planar cells compared to bare GF SCs. The relatively low resistances of SCs may be attributed to improved conductivity and better affinity of the GF/PPy electrodes toward electrolytes. In addition, Bode plots of GF and GF/PPy SCs (Figure 7c,d) indicated phase angles for different cell configurations between −60° and −79° at a frequency of 10 mHz, which is close to the 90° of an ideal capacitor, coinciding with the general RC equivalent circuit for supercapacitors.[50]

CONCLUSION

In summary, a flexible supercapacitor electrode based on a graphite flakes/polypyrrole hybrid structure was fabricated through a simple technique utilizing polymer lapping film as a flexible substrate. The flexible device exhibited good electrochemical performance, with area capacitance of 37 mF cm^{-2} in 1 M H_2SO_4 electrolyte, 23 mF cm^{-2} within an all solid state flexible capacitor, and 6 mF cm^{-2} in planar configuration, with an excellent energy density and power density. This demonstration of GF/PPy SCs shows a great potential application in energy management for flexible and lightweight electronics. Moreover, the fabrication of electrodes over polymer lapping films may greatly contribute to the utilization of patterned rough polymer surfaces as inexpensive flexible substrates.

ASSOCIATED CONTENT

Supporting Information

Additional figures, table, and references. The Supporting Information is available free of charge on the ACS Publications website at DOI: 10.1021/acsami.5b02070.

AUTHOR INFORMATION

Corresponding Author

*E-mail: yukook@dongguk.edu. Phone: +82 2 2260 3709.

Notes

The authors declare no competing financial interest.

ACKNOWLEDGMENTS

The authors would like to acknowledge authorities of Dongguk University—Seoul for their moral and financial support. This research was supported by the National Research Foundation of South Korea (NRF) (No. 2014030484)

REFERENCES

(1) Sun, Y. G.; Rogers, J. A. Inorganic Semiconductors for Flexible Electronics. *Adv. Mater.* **2007**, *19*, 1897−1916.

(2) Cao, Q.; Kim, H.; Pimparkar, N.; Kulkarni, J. P.; Wang, C.; Shim, M.; Roy, K.; Alam, M. A. Medium-Scale Carbon Nanotube Thin-Film Integrated Circuits on Flexible Plastic Substrates. *Nature* **2008**, *454*, 495−500.

(3) Su, F.; Miao, M.; Niu, H.; Wei, Z. Gamma-Irradiated Carbon Nanotube Yarn As Substrate for High- Performance Fiber Supercapacitors. *ACS Appl. Mater. Interfaces* **2014**, *6*, 2553−2560.

(4) Wu, Z. S.; Parvez, K.; Feng, X.; Mullen, K. Graphene-Based In-Plane Micro-Supercapacitors with High Power and Energy Densities. *Nat. Commun.* **2013**, *4*, 2487−2494.

(5) Xu, Y.; Lin, Z.; Huang, X.; Liu, Y.; Huang, Y.; Duan, X. Flexible Solid-State Supercapacitors Based on Three-Dimensional Graphene Hydrogel Films. *ACS Nano* **2013**, *7*, 4042−4049.

(6) Nyholm, L.; Nystrom, G.; Mihranyan, A.; Stromme, M. Toward Flexible Polymer and Paper-Based Energy Storage Devices. *Adv. Mater.* **2011**, *23*, 3751−3769.

(7) Gwon, H.; Hong, J.; Kim, H.; Seo, D. H.; Jeon, S.; Kang, K. Recent Progress on Flexible Lithium Rechargeable Batteries. *Energy Environ. Sci.* **2014**, *7*, 538−551.

(8) Yang, X.; Zhu, J.; Qiu, L.; Li, D. Bioinspired Effective Prevention of Restacking in Multilayered Graphene Films: Towards the Next Generation of High-Performance Supercapacitors. *Adv. Mater.* **2011**, *23*, 2833−2838.

(9) Burke, A. Ultracapacitors: Why, How, and Where is the Technology. *J. Power Sources* **2000**, *91*, 37−50.

(10) Gao, H.; Xiao, F.; Ching, C. B.; Duan, H. Flexible All-Solid-State Asymmetric Supercapacitors Based on Free-Standing Carbon Nanotube/Graphene and Mn_3O_4 Nanoparticle/Graphene Paper Electrodes. *ACS Appl. Mater. Interfaces* **2012**, *4*, 7020−7026.

(11) Yuan, L.; Lu, X. H.; Xiao, X.; Zhai, T.; Dai, J.; Zhang, F.; Hu, B.; Wang, X.; Gong, L.; Chen, J.; Hu, C.; Tong, Y.; Zhou, J.; Wang, Z. L. Flexible Solid-State Supercapacitors Based on Carbon Nanoparticles/MnO_2 Nanorods Hybrid Structure. *ACS Nano* **2012**, *6*, 656−661.

(12) Chen, S.; Xing, W.; Duan, J.; Huc, X.; Qiao, S. Q. Nanostructured Morphology Control for Efficient Supercapacitor Electrodes. *J. Mater. Chem. A* **2013**, *1*, 2941−2954.

(13) Simon, P.; Gogotsi, Y. Materials for Electrochemical Capacitors. *Nat. Commun.* **2008**, *7*, 845−854.

(14) Bi, R. R.; Wu, X. L.; Cao, F. F.; Jiang, L. Y.; Guo, Y. G.; Wan, L. J. Highly Dispersed RuO_2 Nanoparticles on Carbon Nanotubes: Facile Synthesis and Enhanced Supercapacitance Performance. *J. Phys. Chem. C* **2010**, *114*, 2448−2451.

(15) Bai, Y.; Du, M.; Chang, J.; Sun, J.; Gao, L. Supercapacitors with High Capacitance Based on Reduced Graphene Oxide/Carbon Nanotubes/NiO Composite Electrodes. *J. Mater. Chem. A* **2014**, *2*, 3834−3840.

(16) Jin, Y.; Chen, H.; Chen, M.; Liu, N.; Li, Q. Graphene-Patched CNT/MnO_2 Nanocomposite Papers for the Electrode of High-Performance Flexible Asymmetric Supercapacitors. *ACS Appl. Mater. Interfaces* **2013**, *5*, 3408−3416.

(17) Mao, M.; Mei, L.; Wu, L.; Li, Q.; Zhang, M. Facile Synthesis of Cobalt Sulfide/Carbon Nanotube Shell/Core Composites for High Performance Supercapacitors. *RSC Adv.* **2014**, *4*, 12050−12056.

(18) Salunkhe, R. R.; Lin, J.; Malgras, V.; Doub, S. X.; Kim, J. H.; Yamauchi, Y. Large-Scale Synthesis of Coaxial Carbon Nanotube/$Ni(OH)_2$ Composites for Asymmetric Supercapacitor Application. *Nano Energy* **2015**, *11*, 211−218.

(19) Peng, C.; Zhang, S.; Jewell, D.; Chen, G. Z. Carbon Nanotube and Conducting Polymer Composites for Supercapacitors. *Prog. Nat. Sci.* **2008**, *18*, 777−788.

(20) Ramya, R.; Sivasubramaniam, R.; Sangaranarayanan, M. V. Conducting Polymers-Based Electrochemical Supercapacitors-Progress and Prospects. *Electrochim. Acta* **2013**, *101*, 109−129.

(21) Liu, X.; Shang, P.; Zhang, Y.; Wang, X.; Fan, Z.; Wang, B.; Zheng, Y. Three-Dimensional and Stable Polyaniline-Grafted Graphene Hybrid Materials for Supercapacitor Electrodes. *J. Mater. Chem. A* **2014**, *2*, 15273−15278.

(22) Mykhailiv, O.; Imierska, M.; Petelczyc, M.; Echegoyen, L.; Brzezinska, M. E. P. Chemical versus Electrochemical Synthesis of

DOI: 10.1021/acsami.5b02070
ACS Appl. Mater. Interfaces 2015, 7, 13405−13414

Carbon Nano-Onion/Polypyrrole Composites for Supercapacitor Electrodes. *Chem.—Eur. J.* **2015**, *21*, 5783−5793.
(23) Snook, G. A.; Kao, P.; Best, A. S. Conducting-Polymer-Based Supercapacitor Devices and Electrodes. *J. Power Sources* **2011**, *196*, 1−12.
(24) Yang, C.; Liu, P.; Wang, T. Well-Defined Core-Shell Carbon Black/Polypyrrole Nanocomposites for Electrochemical Energy Storage. *ACS Appl. Mater. Interfaces* **2011**, *3*, 1109−1114.
(25) Li, X.; Zhitomirsky, I. Electrodeposition of Polypyrrole-Carbon Nanotube Composites for Electrochemical Supercapacitors. *J. Power Sources* **2013**, *221*, 49−56.
(26) Bora, C.; Sharma, J.; Dolui, S. Polypyrrole/Sulfonated Graphene Composite as Electrode Material for Supercapacitor. *J. Phys. Chem. C* **2014**, *118*, 29688−29694.
(27) Chen, T.; Dai, L. Flexible Supercapacitors Based on Carbon Nanomaterials. *J. Mater. Chem. A* **2014**, *2*, 10756−10775.
(28) Hu, L.; Cui, Y. Energy and Environmental Nanotechnology in Conductive Paper and Textiles. *Energy Environ. Sci.* **2012**, *5*, 6423−6435.
(29) Fu, Y.; Cai, X.; Wu, H.; Lv, Z.; Hou, S.; Peng, M.; Yu, X.; Zou, D. Fiber Supercapacitors Utilizing Pen Ink for Flexible/Wearable Energy Storage. *Adv. Mater.* **2012**, *24*, 5713−5718.
(30) Zhang, C.; Yin, H.; Han, M.; Dai, Z.; Pang, H.; Zheng, Y.; Lan, Y.; Bao, J.; Zhu, J. Two-Dimensional Tin Selenide Nanostructures for Flexible All-Solid-State Supercapacitors. *ACS Nano* **2014**, *8*, 3761−3770.
(31) Choi, C.; Lee, J. A.; Choi, A. Y.; Kim, Y. T.; Lepro, X.; Lima, M. D.; Baughman, R. H.; Kim, S. J. Flexible Supercapacitor Made of Carbon Nanotube Yarn with Internal Pores. *Adv. Mater.* **2014**, *26*, 2059−2065.
(32) Yoo, J. J.; Balakrishnan, K.; Huang, J.; Meunier, V.; Sumpter, B. G.; Srivastava, A.; Conway, M.; Reddy, A. L. M.; Yu, J.; Vajtai, R.; Ajayan, P. M. Ultrathin Planar Graphene Supercapacitors. *Nano Lett.* **2011**, *11*, 1423−1427.
(33) Naoi, K.; Naoi, W.; Aoyagi, S.; Miyamoto, J. I.; Kamino, T. New Generation Nanohybrid Supercapacitor. *Acc. Chem. Res.* **2013**, *46*, 1076−1083.
(34) Chen, G. Z. Understanding Supercapacitors Based on Nanohybrid Materials with Interfacial Conjugation. *Prog. Nat. Sci. Mater. Int.* **2013**, *23*, 245−255.
(35) Renolds, J. R.; Warren, L. F.; Marcy, H. O. Long-Term Switching Stability of Polypyrrole. *Synth. Met.* **1994**, *68*, 71−77.
(36) Guanggui, C.; Jianning, D.; Zhongqiang, Z.; Zhiyong, L.; Huasheng, P. Study on the Preparation and Multiproperties of the Polypyrrole Films Doped with Different Ions. *Surf. Interface Anal.* **2012**, *44*, 844−850.
(37) Kumar, A.; Singh, R. K.; Singh, H. K.; Srivastava, P.; Singh, R. Enhanced Capacitance and Stability of p-Toluenesulfonate Doped Polypyrrole/Carbon Composite for Electrode Application in Electrochemical Capacitors. *J. Power Sources* **2014**, *246*, 800−807.
(38) Mollahosseini, A.; Noroozian, E. Electrodeposition of a Highly Adherent and Thermally Stable Polypyrrole Coating on Steel from Aqueous Polyphosphate Solution. *Synth. Met.* **2009**, *159*, 1247−1254.
(39) Wang, J.; Mo, X.; Ge, D.; Tian, Y.; Wang, Z.; Wang, S. Polypyrrole Nanostructures Formed by Electrochemical Method on Graphite Impregnated with Paraffin. *Synth. Met.* **2006**, *156*, 514−518.
(40) Zhou, C.; Zhang, Y.; Li, Y.; Liu, J. Construction of High-Capacitance 3D CoO@ Polypyrrole Nanowire Array Electrode for Aqueous Asymmetric Supercapacitor. *Nano Lett.* **2013**, *13*, 2078−2085.
(41) Bettini, L. G.; Galluzzi, M.; Podesta, A.; Milani, P.; Piseri, P. Planar Thin Film Supercapacitor Based on Cluster-Assembled Nanostructured Carbon and Ionic Liquid Electrolyte. *Carbon* **2013**, *59*, 212−220.
(42) Kim, D.; Lee, G.; Kim, D.; Ha, J. S. Air-Stable, High-Performance, Flexible Microsupercapacitor with Patterned Ionogel Electrolyte. *ACS Appl. Mater. Interfaces* **2015**, *7*, 4608−4615.
(43) Peng, L.; Peng, X.; Liu, B.; Wu, C.; Xie, Y.; Yu, G. Ultrathin Two-Dimensional MnO_2/Graphene Hybrid Nanostructures for High-Performance, Flexible Planar Supercapacitors. *Nano Lett.* **2013**, *13*, 2151−2157.
(44) Wu, Z. S.; Parvez, K.; Feng, X.; Mullen, K. Graphene-Based In-Plane Micro-Supercapacitors with High Power and Energy Densities. *Nat. Commun.* **2013**, *4*, 2487.
(45) Wang, J. G.; Yang, Y.; Huang, Z. H.; Kang, F. A High-Performance Asymmetric Supercapacitor Based on Carbon and Carbon-MnO_2 Nanofiber Electrodes. *Carbon* **2013**, *61*, 190−199.
(46) Wang, X.; Liu, B.; Wang, Q.; Song, W.; Hou, X.; Chen, D.; Cheng, Y.; Shen, G. Three-Dimensional Hierarchical $GeSe_2$ Nanostructures for High Performance Flexible All-Solid-State Supercapacitors. *Adv. Mater.* **2013**, *25*, 1479−1486.
(47) Yuan, L.; Yao, B.; Hu, B.; Huo, K.; Chen, W.; Zhou, J. Polypyrrole-Coated Paper for Flexible Solid-State Energy Storage. *Energy Environ. Sci.* **2013**, *6*, 470−476.
(48) Zheng, G.; Hu, L.; Wu, H.; Xie, X.; Cui, Y. Paper Supercapacitors by a Solvent-Free Drawing Method. *Energy Environ. Sci.* **2011**, *4*, 3368−3373.
(49) Kim, J. H.; Kang, S. H.; Zhu, K.; Kim, J. Y.; Neale, N. R.; Frank, A. J. Ni−NiO Core−shell Inverse Opal Electrodes for Supercapacitors. *Chem. Commun.* **2011**, *47*, 5214−5216.
(50) Fabio, A. D.; Giorgi, A.; Mastragostino, M.; Soavi, F. Carbon-Poly(3-methylthiophene) Hybrid Supercapacitors. *J. Electrochem. Soc.* **2001**, *148*, A845−A850.

DOI: 10.1021/acsami.5b02070
ACS Appl. Mater. Interfaces 2015, 7, 13405−13414